



1

1 **A thicker, rather than thinner, East Antarctic Ice Sheet plateau** 2 **during the Last Glacial Maximum**

3 Cari Rand¹, Richard S. Jones¹, Andrew N. Mackintosh¹, Brent Goehring², Kat Lilly³

4 ¹Securing Antarctica's Environmental Future, School of Earth, Atmosphere and Environment, Monash
5 University, Wellington Road, Clayton, Melbourne, Victoria 3800, Australia

6 ²Los Alamos National Laboratory, Bikini Atoll Road, Los Alamos, New Mexico 87545, USA

7 ³RSC, PO Box 5647, Dunedin, New Zealand

8 *Correspondence to:* Cari Rand (cari.rand@monash.edu)

9 **Abstract.** In this study, we present a surface-exposure chronology of past ice-thickness change derived from *in-*
10 *situ* cosmogenic-¹⁴C dating at a site on the edge of the East Antarctic plateau, 380 km inland from the Antarctic
11 coastline. Our knowledge of how the Antarctic ice sheet has responded to Quaternary climate change relies on a
12 combination of geological data and ice-sheet modeling. At the Last Glacial Maximum (LGM), observations and
13 models suggest that increased ice-sheet volume was accommodated by thicker ice near the coast and grounding-
14 line advance towards the continental-shelf edge. In contrast, the ice sheet interior maintained a relatively stable
15 thickness until present, with ice-core evidence even suggesting thinner ice relative to today. However, the
16 magnitude of these thickness changes, and the location dividing thicker versus thinner ice at the LGM is poorly
17 constrained. Geological reconstructions of past ice thickness in Antarctica mostly come from surface-exposure
18 data using cosmogenic nuclides that are relatively insensitive records of ice-cover changes on timescales of tens
19 of thousands of years. This can lead to inaccurate records of LGM ice thickness, particularly towards the East
20 Antarctic plateau, where cold-based non-erosive ice may inhibit bedrock erosion. Samples saturated with ¹⁴C at
21 1912 m a.s.l. indicate that the summit of Nunatak 1921 was exposed during the LGM, while unsaturated samples
22 indicate that thinning subsequently occurred, with some (25-45%) post-LGM thinning recorded at ~15-11 ka and
23 most (55-75%) recorded during the Holocene. These results imply that at least part of the interior East Antarctic
24 Ice Sheet (EAIS) was thicker at the LGM than it is now, and that gradual ice-sheet thinning began ~15 ka. Ice-
25 sheet models that do not account for this thickness change would inaccurately characterize the LGM geometry of
26 the EAIS and underestimate its contributions to deglacial sea-level rise.

27 **1 Introduction**

28 The East Antarctic Ice Sheet (EAIS) is the largest contiguous mass of ice on Earth (Rignot *et al.*, 2019). Loss of
29 ice to melting and calving is predicted to be offset by increases in snow accumulation over the coming century,
30 but beyond 2100 CE, the ice sheet is expected to lose mass and contribute to sea-level rise (Stokes *et al.*,
31 2022). Characterizing past changes of the EAIS is necessary for several reasons:

- 32 1. Satellite observations of Antarctic glaciers extend back only to the 1960s, so other records of past ice-
33 sheet states are needed in order to reliably distinguish long-term trends from natural variability (Hanna
34 *et al.*, 2020; Jones *et al.*, 2022);



2

- 35 2. Geodetic data used to estimate modern ice-mass changes must be corrected for glacial isostatic
36 adjustment (e.g., Coulon *et al.*, 2021), the magnitude of which is dependent on the past configuration of
37 the ice sheet;
- 38 3. Determining the magnitude and timing of ice loss can identify or exclude potential sources of meltwater
39 input to oceans during past periods of rapid sea-level rise (e.g., Lin *et al.*, 2021); and
- 40 4. Numerical models informed by records of past ice-sheet change are used to estimate the future
41 contributions to sea-level rise (e.g., DeConto *et al.*, 2021).

42 However, reconstructing the geometry of the EAIS is challenging. Evidence of past ice thickness comes from
43 radar, ice-core and geological data, which are sparse owing to the remoteness of East Antarctica, the large area of
44 the ice sheet, and the sparsity of ice-free areas. Furthermore, different records of LGM ice thickness are often in
45 disagreement with one another.

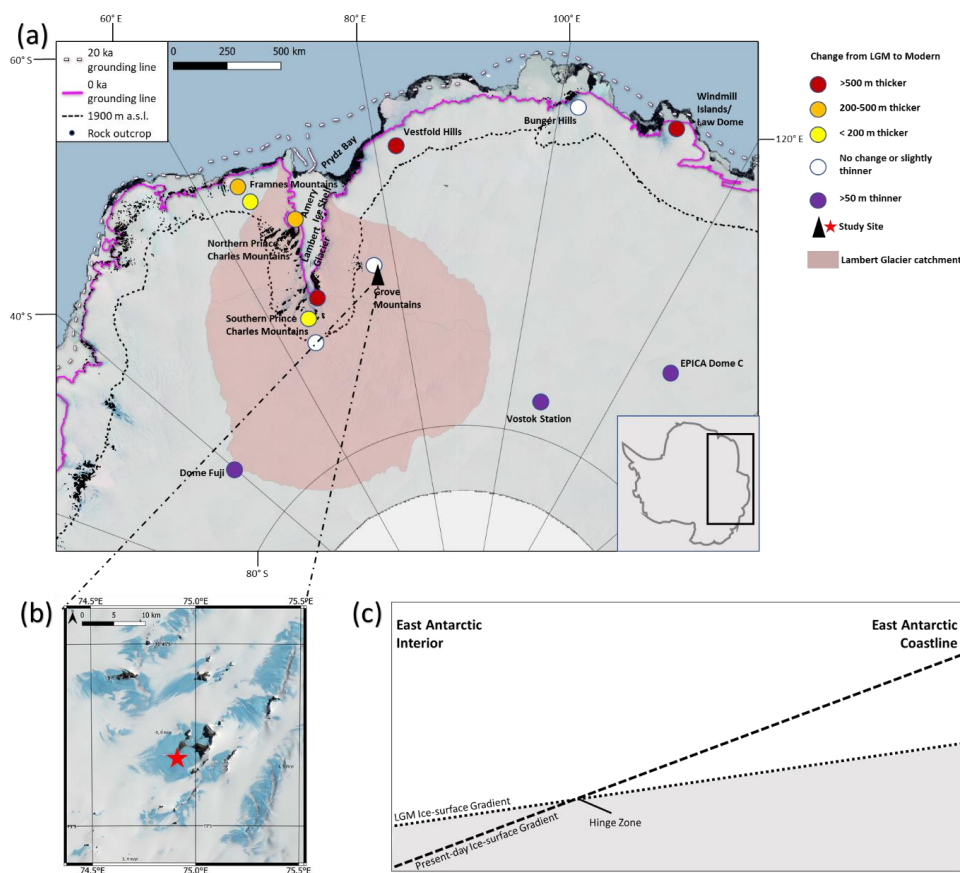
46 During the Last Glacial Maximum (LGM), at approximately 20 ka, available evidence points towards a more
47 extensive but shallower-gradient ice sheet (Mackintosh *et al.*, 2014). Dated acid-insoluble organic matter in
48 sediments from the East Antarctic coast indicate that the EAIS advanced to the edge of the continental shelf in
49 most locations during the LGM (Bentley *et al.*, 2014), with constraints from cosmogenic ^{10}Be and ^{26}Al indicating
50 the presence of ice near the coast that was thicker than it is now (e.g., Mackintosh *et al.*, 2007; White *et al.*, 2011;
51 Yamane *et al.*, 2011). Meanwhile, snow-accumulation rates interpolated between ice domes indicate a thinner ice
52 sheet across the East Antarctic plateau (Buizert *et al.*, 2021) at the LGM. A “hinge zone” thus likely existed
53 between thicker ice at the coast and thinner ice in the interior during the LGM relative to today (Bockheim *et al.*,
54 1989; Andersen *et al.*, 2023), but the location of this transition point across East Antarctica is unclear. Cosmogenic
55 ^{10}Be and ^{26}Al ages from ice-free areas on the edge of the East Antarctic plateau such as the Grove Mountains or
56 southern Prince Charles Mountains are older than the LGM (e.g., Lilly *et al.*, 2010; White *et al.*, 2011), implying
57 no change since or slightly thinner ice in these locations at the LGM (**Fig. 1**).

58 Yet existing cosmogenic-nuclide data from regions of cold-based non-erosive ice may not provide reliable
59 constraints on LGM ice thickness. Many samples have apparently pre-LGM and inconsistent ^{10}Be and ^{26}Al
60 exposure ages, indicating nuclides inherited from previous periods of exposure (Balco *et al.*, 2014). Due to the
61 short half-life of *in situ* ^{14}C (5.7 kyr), its concentration decays quickly when shielded (e.g., when covered by ice;
62 Goehring, Balco, *et al.*, 2019); this makes *in situ* ^{14}C a useful tool for investigating post-LGM glacial history
63 (Nichols, 2022).

64



3



65

66 **Figure 1: Constraints on central East Antarctic ice thickness at the Last Glacial Maximum (LGM).** (a)
 67 **Inferred LGM-to-present ice-thickness differences near Lambert Glacier.** Dashed black line shows the 1900
 68 **m a.s.l. contour** (Liu *et al.* 2015), the elevation of our sampled nunatak. This line represents the most interior
 69 **geological evidence and reflects a potential hinge zone** between coastal and interior LGM-ice-thickness
 70 **change.** Elements of this map were provided by the Quantarctica 3 GIS package provided by the Norwegian
 71 **Polar Institute** (Matsuoka *et al.*, 2018), including ice-free areas (Burton-Johnson *et al.*; 2016), the current
 72 **Antarctic-ice-sheet grounding line** (Bindschadler *et al.*, 2011), and the inferred East Antarctic grounding
 73 **line 20 ka** (Bentley *et al.*, 2014). Red-shaded ice indicates the extent of the catchment of Lambert Glacier
 74 **(Zwally *et al.*, 2012).** LGM thickness data for this figure come from Buizert *et al.* (2021; Dome Fuji and
 75 **EPICA Dome C)**, Lilly *et al.* (2010; Grove Mountains), Mackintosh *et al.* (2007; Framnes Mountains),
 76 **Mackintosh *et al.* (2014)** and references therein (Bunger Hills, Law Dome, Vestfold Hills, Vostok Station,
 77 **and Windmill Islands)**, and White *et al.* (2011; Prince Charles Mountains). (b) Satellite view of the study
 78 **area with the sampled nunatak (Nunatak 1921).** Bedrock and erratic samples were collected in a transect
 79 **extending from the modern ice surface to nunatak summit.** (c) Diagram illustrating the concept of a “hinge
 80 **zone” in ice-thickness change.** Image shows hypothetical vertically exaggerated cross-sections of the East
 81 **Antarctic Ice Sheet at the LGM (dotted line) and present day (dashed line).** If coastal ice thins and interior



4

82 **ice thickens after the LGM, the modern ice-surface profile would intersect the LGM surface profile**
83 **somewhere in the middle; this intersection is the “hinge zone”, at which ice there has been no net change in**
84 **ice thickness since the LGM. LGM-thickness reconstructions in White *et al.* (2011) and Lilly *et al.* (2010)**
85 **placed the “hinge zone” in areas equivalent to a present-day ice-surface elevation of ~1900 m a.s.l.**

86

87 In this study, we aim to constrain how far inland the EAIS was thicker at the LGM than it is at present by testing
88 previously-measured samples at a key site in the ice sheet interior using *in situ* ^{14}C . Rocks exposed since before
89 the LGM should be saturated with ^{14}C , meaning that the rates of *in situ* ^{14}C production and decay are equal (a state
90 which requires 3-5 half-lives of exposure to reach; Dunai, 2010). Conversely, exposed rocks with less-than-
91 saturated concentrations of ^{14}C from a site in East Antarctica imply that those samples were covered at some time
92 since the LGM by a thicker-than-present EAIS that subsequently thinned. The concentration of a cosmogenic
93 nuclide in a sample will remain at secular equilibrium indefinitely unless disturbed by cover, erosion, or transport;
94 thus, only a minimum age can be assigned to saturated samples. Measuring samples from an elevation transect
95 with *in situ* ^{14}C thus allows us to reevaluate the ice-thickness history at the site: the ice must have been thick
96 enough to cover at least the highest-elevation unsaturated sample, and had to have been that thick within the time
97 it would have taken for the ^{14}C concentration of that sample to reach saturation again.

98 1.1 Study Area

99 The Grove Mountains are well located to assess how far inland the EAIS was thicker at the LGM than it is at
100 present and whether previously measured concentrations of ^{10}Be and ^{26}Al from this site likely reflect a component
101 of nuclides inherited from a previous period of exposure. These isolated nunataks are located ~200 km upstream
102 of the main trunk of Lambert Glacier and ~400 km inland/south of the Antarctic coast (**Fig. 1**) and are the most
103 interior ice-free area in this region. The summits of the nunataks rise 100-200 m above the modern ice surface
104 (~1800 m a.s.l.), providing the potential to record past EAIS-thickness changes. Ice flows slowly ($<5\text{ m yr}^{-1}$) to
105 the west-northwest between these nunataks (Rignot *et al.*, 2011).

106 At Nunatak 1921, evidence of past ice cover is apparent from the occurrence of felsic cobbles atop very weathered
107 orthogneiss bedrock (Lilly, 2008). Given the sparsity of outcrops and non-channelized nature of ice flow in the
108 interior EAIS, we are not able to identify the provenance of these cobbles beyond stating that they are not locally
109 derived (i.e. they are erratics).

110 2 Methods

111 Here we reanalyze samples first presented in Lilly *et al.* (2010), which were collected from the Grove Mountains
112 for ^{10}Be and ^{26}Al analysis as part of a study of the long-term glacial history of the region. Measurements of ^{10}Be
113 and ^{26}Al were carried out in 2004 at the ANTARES Accelerator Mass Spectrometry facility. Nuclide
114 concentrations below saturation were recorded for all samples, indicating 40-700 kyr of exposure since the
115 bedrock was last reset. For full details, see Lilly (2008) and Lilly *et al.* (2010).

116 The samples were collected in an elevation transect from the present-day ice surface on the upstream face of
117 Nunatak 1921 in 2003/4 and 2004/5 (Lilly *et al.*, 2010; **Table 1**). Pairs of bedrock and erratic samples showed no
118 evidence of post-depositional movement, cover by sediments, or subaerial erosion. Samples were preferentially



5

119 collected from ridgetops to minimize the chances of shielding by snow. As neither plucking scars nor glacial striae
120 were observed at the site (Lilly *et al.*, 2010), indicating low or negligible rates of subglacial erosion, we anticipate
121 that the existing ^{10}Be and ^{26}Al concentrations do not accurately record LGM ice thickness.
122 To provide a test of LGM ice thickness, we carried out *in situ* ^{14}C analysis on ten of these samples that form a
123 transect covering 96 m of elevation (1825-1921 m a.s.l.). Seven of the samples (GR01, GR03, GR04, GR06,
124 GR07, GR13, and GR18) were erratic cobbles. The remaining three (GR12, GR15, and GR21) were bedrock
125 samples.
126
127



6

128 **Table 1: Sample locations**

Sample ID	Elevation (m a.s.l.)	Elevation above modern ice surface (m)	Latitude (degrees S)	Longitude (degrees E)	Thickness (cm)	Topographic shielding	Lithology
GR01	1832	7	72.9115	74.9096	2	0.985	Felsic metamorphic
GR03	1854	29	72.9115	74.9079	2	0.992	Quartzite
GR04	1870	45	72.9110	74.9067	2	1.000	Quartzite
GR06	1894	69	72.9099	74.9044	2	0.998	Fine-grained felsic
GR07	1921	96	72.9088	74.9045	2	1.000	Quartzite
GR12*	1825	0	72.9112	74.9097	2	0.985	Orthogneiss
GR13	1839	14	72.9115	74.9094	2	0.993	Unknown
GR15*	1847	22	72.9115	74.9088	3	0.993	Orthogneiss
GR18	1873	48	72.9108	74.9061	4	1.000	Vein quartz
GR21*	1912	87	72.9088	74.9045	3	0.999	Orthogneiss

129 **A density of 2.7 g cm⁻³ is assumed for all samples. Bedrock-sample IDs are marked with an asterisk; all**
130 **other samples were erratic cobbles.**

131

132 Quartz was isolated through physical and chemical processing at the Tulane University Cosmogenic Nuclides
133 Laboratory (TUCNL; Goehring *et al.*, 2019). Whole samples were crushed and milled, then all samples were
134 sieved to select their 125-500-micron fractions. Sieved samples were then rinsed with tap water to remove clay-
135 sized grains. A roller-type magnetic separator was then used to remove magnetic minerals. Froth flotation was
136 used to separate quartz and feldspar grains, followed by etching for at least two days in 5% HF/HNO₃ on a shaker
137 table and at least two days in a sonicator in 1% HF/HNO₃ in order to remove adsorbed carbon species (Nichols
138 and Goehring, 2019).

139 Following the isolation and purification, 0.6-5 g aliquots were separated from the cleaned quartz for ¹⁴C extraction.
140 Before extraction, each aliquot was sonicated in 50% HNO₃ for 0.5 hr, then rinsed with Type I water and dried
141 overnight in a vacuum oven. The dried quartz was then loaded into a LiBO₂-flux-containing Pt crucible and step
142 heated in O₂ for 0.5 hr at 500 °C and 3 hr at 1,100 °C in the Tulane University Carbon Extraction and
143 Graphitization System. Carbon species released were oxidized to CO₂ over hot quartz, then cryogenically purified,
144 collected, and diluted with ¹⁴C-free CO₂. An aliquot of this gas was separated for δ¹³C analysis and the remainder
145 graphitized via Fe-catalyzed H₂ reduction. For further details, see the method of Goehring *et al.* (2019).
146 Concentrations of ¹⁴C were then measured at the National Ocean Sciences Accelerator Mass Spectrometry facility
147 at the Woods Hole Oceanographic Institution, and data reduction followed Hippe and Lifton (2014).

148 A blank value of 58,000 ± 3,110 atoms was subtracted from the total measured atoms from each sample; this value
149 represents the continually updated mean value of process blanks run at the TUCNL since April, 2016 (Goehring
150 *et al.*, 2019). This blank-corrected measurement was divided by the run mass to determine the ¹⁴C concentration
151 of each sample. Exposure ages were calculated using the “LSDn” nuclide-specific production rate scaling scheme
152 of Lifton *et al.* (2014). The production rate of *in-situ* ¹⁴C was calibrated using the CRONUS-A interlaboratory
153 comparison material (Goehring *et al.*, 2019). The CRONUS-A material is assumed to be saturated with *in-situ* ¹⁴C
154 based on geological observations indicating that its collection site has not been covered in the last 11.3 Myr
155 (Goehring *et al.*, 2019; Nichols *et al.*, 2019). Repeated measurements of CRONUS-A material at the TUCNL



7

156 show ~6% variation in ^{14}C concentrations; thus, we use a minimum uncertainty equal to 6% of the calculated ^{14}C
157 concentration of our samples for exposure-age calculation (**Table 2**).

158

159 **Table 2: Sample ^{14}C concentrations and exposure ages**

Sample number	$[^{14}\text{C}]$ (10^5 atoms g^{-1})	^{14}C Age (ka)	Internal ^{14}C -age uncertainty (ka)	External ^{14}C -age uncertainty (ka)
GR01	0.86 ± 0.08	1.021	0.098	0.100
GR03	2.80 ± 0.17	4.023	0.312	0.324
GR04	5.41 ± 0.33	11.004	1.387	1.442
GR06	6.20 ± 0.38	14.660	2.452	2.549
GR07	8.05 ± 0.49	Saturated	N/A	N/A
GR12(BR)	1.14 ± 0.07	1.393	0.091	0.095
GR13	1.59 ± 0.10	2.005	0.136	0.142
GR15(BR)	0.15 ± 0.01	0.019	0.013	0.013
GR18	5.47 ± 0.33	11.600	1.530	1.590
GR21(BR)	7.78 ± 0.11	Saturated	N/A	N/A

160 **All measurements of ^{14}C atoms per sample corrected by subtracting a 0.58 ± 0.31 atom blank prior to**
161 **concentration calculation. “Internal” ^{14}C -age uncertainty includes only instrumental uncertainty.**
162 **“External” ^{14}C -age uncertainty includes both instrumental and production-rate uncertainties.**

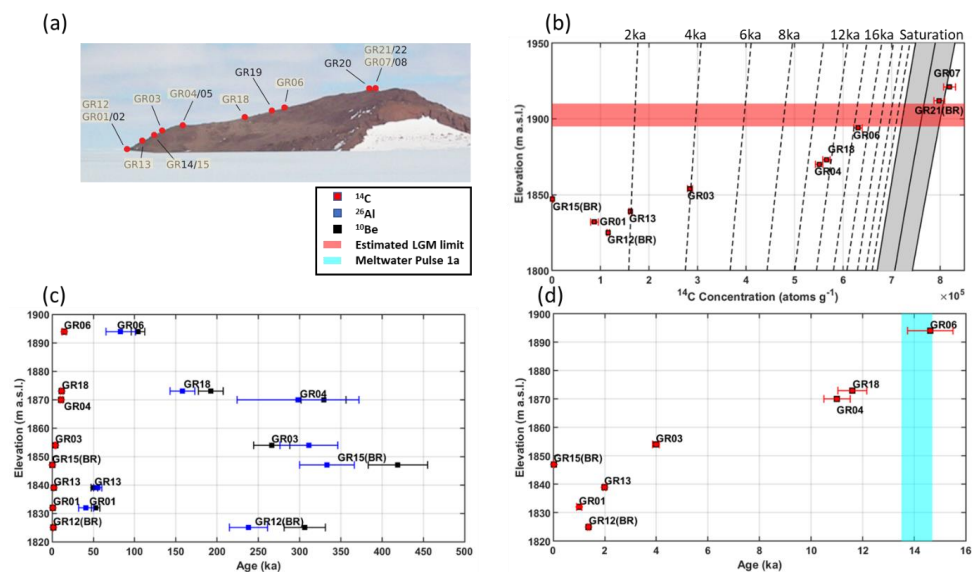
163 3 Results

164 Our samples have ^{14}C concentrations between $15 \pm 0.96 \times 10^3$ atoms g^{-1} (GR15) and $805 \pm 48.3 \times 10^3$ atoms g^{-1}
165 (GR07). The sample with the lowest concentration has an exposure age of 0.02 ± 0.01 ka, and the samples with
166 the highest concentrations are saturated (**Table 2**). These exposure ages are 40 ± 9 (GR01) to 262 ± 22 kyr (GR03)
167 less than ^{10}Be and ^{26}Al concentrations from each sample (for full sample-measurement details, see **Table S1**).
168 Samples form a thinning transect with concentrations and ages mostly increasing monotonically with elevation
169 (**Fig. 2**). There are however two exceptions, both low-elevation bedrock samples (GR15 and GR12). We suspect
170 that the sites of these two samples may have been covered by snow, other sediment, or a boulder that moved
171 within the last millennium.

172



8



173

174

175

176

177

178

179

180

181

182

183

184

185

186

187

188

Figure 2: Sample nuclide concentrations and exposure ages. The current ice surface at this site is roughly coincident with the elevation of sample GR12. (a) Locations of samples noted on a photograph of the south face of Nunatak 1921. IDs of samples from which ^{14}C was measured in this study are highlighted. This image modified from Lilly *et al.* (2010). (b) ^{14}C concentrations plotted against elevation. Isochrons (dotted lines) show corresponding exposure ages at each elevation. Tilted vertical gray band to right represents the saturation error envelope. Samples GR07 and GR21 are saturated, indicating >25 kyr of exposure and implying the summit of the nunatak was exposed during the LGM. Horizontal red band indicates the range of possible LGM ice-surface elevations limited by the elevations of GR06, the highest-elevation unsaturated sample, and GR21, the lowest-elevation saturated sample. Samples GR15 and GR21 are out of stratigraphic order and considered outliers. (c) Sample exposure ages plotted against elevation, calculated from concentrations of ^{14}C (this work) and ^{26}Al and ^{10}Be (Lilly *et al.*, 2010). Note the younger exposure ages calculated from ^{14}C . (d) As plot (c), but only showing ^{14}C exposure ages for the last 16 ka. Light blue bar indicates the timing of meltwater pulse 1a (Deschamps *et al.*, 2012). Samples GR07 and GR21 are saturated with ^{14}C and thus omitted from this plot. See the Supplementary tables for all sample information, nuclide concentrations and calculated exposure ages.

189

190

191

192

193

194

195

If the ice-sheet thickness was similar to or thinner than at present in the vicinity of the Grove Mountains at the LGM, our samples would be saturated with ^{14}C . However, our samples show a clear trend of increasing ^{14}C concentrations with elevation (Fig. 2). Only two samples (GR07 and GR21, Table 2) show evidence of saturation, both near the summit of the nunatak. These results thus show that ice was thicker at the LGM than at present in the Grove Mountains but not sufficiently thick as to override the summits (at least neither lengthily nor deeply enough to allow nuclide concentrations in these samples to decay below saturation).



9

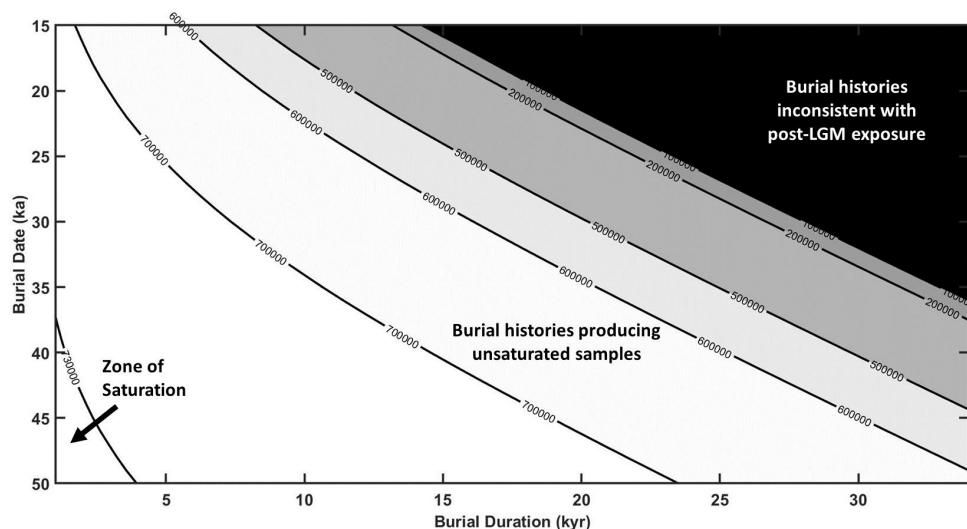
196 The LGM ice surface must have been between the lowest of our saturated and highest of our unsaturated samples,
197 corresponding to an elevation between 1894 and 1912 m a.s.l. This equates to ice 63-87 m thicker at the LGM
198 than at present, with subsequent thinning.
199 Additionally, exposure ages calculated from ^{14}C concentrations allow us to infer a simple thinning history at
200 Nunatak 1921. The highest unsaturated sample (GR06) provides a minimum post-LGM age for the onset of
201 thinning at the site of 14.9 ± 1.0 ka (**Fig. 2, Table 2**). Up to 18 m (21-29%) of thinning could have occurred before
202 and up to 21 m (24-33%) during meltwater pulse 1a (MWP-1a; **Fig. 2(b)**) assuming a linear thinning history, but
203 the potential for glacial overshoot, whereby the glacier thins beyond its new equilibrium thickness and
204 subsequently rethickens, makes these minimum estimates. Most post-LGM thinning (55-70%) is recorded during
205 the Holocene (the last 11.7 ka; Walker *et al.*, 2009). Based on our lowest-elevation sample (GR12), which was
206 collected less than 1 m above the current ice surface (~1820 m a.s.l.), the present-day ice thickness was reached
207 at 1.4 ± 0.1 ka (**Tables 1 & 2**).

208 **4 Discussion**

209 New exposure ages calculated from *in situ* ^{14}C concentrations allow us to revise the history of the EAIS at this
210 site. The combination of saturated and unsaturated samples in the Grove Mountains shows that the highest peaks
211 were exposed during the LGM, yet the ice sheet was modestly thicker (up to 87 m) here at the LGM than at
212 present, contrary to previous ice-thickness data at this site and reconstructions of the interior EAIS at the LGM
213 (e.g. Lilly *et al.*, 2010; Buizert *et al.*, 2021).
214 Longer-lived nuclides from our samples (^{10}Be and ^{26}Al) do not show saturation (Lilly *et al.*, 2010) but the high
215 contribution of inherited nuclides from pre-LGM exposure prevents an accurate test of the LGM ice thickness and
216 reconstruction of the post-LGM thinning history. Our ^{14}C data indicate that ice cover occurred at this site and the
217 period of cover was long enough to allow ^{14}C concentrations in our samples to decay. The summit of the nunatak
218 was either uncovered or only covered briefly or shallowly ($\lesssim 10$ m) enough for the two summit samples to become
219 re-saturated with ^{14}C during the Holocene (**Fig. 3**). Following the LGM, the flanks of the nunatak were re-exposed,
220 and thinning progressed through to the Late Holocene.
221



10



222

223

Figure 3: Burial-history contour plot. Contours show ^{14}C concentrations resulting from glacial histories with one episode of burial. For legibility, only concentrations corresponding to saturation and sample concentrations measured in this study are shown, and concentrations are rounded down to the nearest 10^5 atoms g^{-1} (10^4 atoms g^{-1} in the case of the saturation contour). Sample contour affiliations are as follows: GR15 and GR01: 0 atoms g^{-1} ; GR12 and GR13: 1×10^5 atoms g^{-1} ; GR03: 2×10^5 atoms g^{-1} ; GR04 and GR18: 5×10^5 atoms g^{-1} ; GR06: 6×10^5 atoms g^{-1} ; GR21: 7×10^5 atoms g^{-1} . For precise sample concentrations, see Table 2. The black-shaded part of the graph shows histories that require glacial burial after 15 ka, inconsistent with the 14.9 ka exposure of GR06. The grey-shaded part of the graph shows histories that would result in sample GR21 being unsaturated with ^{14}C . The unshaded portion of the graph shows the uncertainty window of a saturated sample at this latitude and elevation (72.9088°S , $1,912$ m a.s.l.; see Table 1). Only the lesser end of the saturation window is consistent with any significant degree of burial under enough ice to effectively stop production (~ 10 m). Sample GR21 plots off the bottom-left corner of this figure; its ^{14}C concentration ($7.78\text{E}+05$ atoms g^{-1} , see Table 1) is inconsistent with any episode of burial longer than 1 kyr in the last 50 ka, indicating constant exposure since the LGM.

237

238

Direct constraints from cosmogenic ^{10}Be and ^{26}Al show evidence of the ice being thicker near the Antarctic coast at the LGM than at present (e.g., Mackintosh *et al.*, 2007; White *et al.*, 2011), but exposure ages derived from the same nuclides from interior sites such as the Grove Mountains pre-date the LGM (Lilly *et al.*, 2010). While we cannot rule out the thicker-than-present ice at the Grove Mountains being an entirely localized phenomenon, we suggest based on the application of ^{14}C in this study and other Antarctic studies (e.g., Nichols *et al.*, 2019; White *et al.*, 2011; Fogwill *et al.*, 2014; Hillebrand *et al.*, 2021) that at least some previous reconstructions of LGM ice thickness based on longer-lived nuclides (e.g. ^{10}Be and ^{26}Al) away from the coast and fastest-flowing parts of East Antarctica may be inaccurate.

246

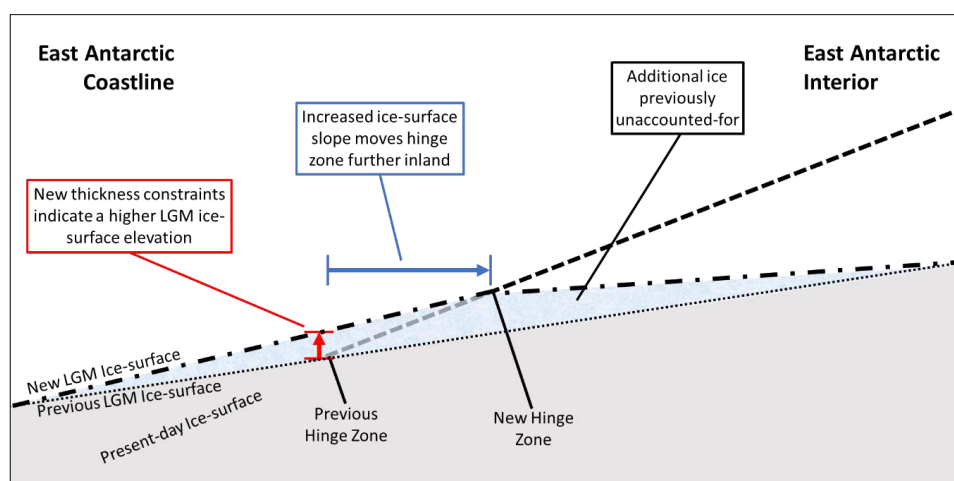
Our new chronology indicates that records of thicker-than-present ice near the East Antarctic coast at the LGM may be representative of ice thicknesses further into the interior than previous reconstructions suggest

247



11

248 (Mackintosh *et al.*, 2014). Cosmogenic dating and geomorphological evidence from elsewhere in the Lambert
249 Glacier catchment support a low-angle ice stream surface at the LGM, with ice 160 m thicker at the most upstream
250 site in the Prince Charles Mountains (Mt. Ruker), and at least 250 m and up to 800 m thicker at sites closer to the
251 coast (White *et al.*, 2011; **Fig. 1**). The “hinge zone” between interior and coastal change, where the LGM ice
252 thickness was the same as today, was proposed to be at ~1900-2000 m a.s.l. based on the available evidence at
253 the Prince Charles Mountains and Grove Mountains (Mackintosh *et al.*, 2014). A thicker-than-present EAIS at
254 the Grove Mountains during the LGM therefore indicates that this “hinge zone” lies further inland, increasing the
255 amount of LGM ice volume across much of the ice sheet (**Fig. 4**).
256



257
258 **Figure 4: Implications of new LGM ice thickness constraints on the East Antarctic “hinge zone”.** Modified
259 from Fig. 1(c), the diagram shows hypothetical vertically exaggerated cross-sections of the East Antarctic
260 Ice Sheet at the present day (dashed line), and at the LGM based on previous evidence (dotted line) and
261 accounting for our data (dot-dashed line). Our results indicate that ice at the Grove Mountains (near the
262 approximate elevation previously considered the “hinge zone”) was ~70 m thicker than it is today.
263 Assuming that LGM ice-thickness estimates near the coast are accurate, this necessitates a steeper coastal
264 ice-surface slope to accommodate the increased thickness at the Grove Mountains (and a shallower East
265 Antarctic plateau ice-surface slope if the LGM ice-thickness estimates in the interior are accurate), moving
266 the “hinge zone” further into the interior. The exact gradients of these slopes and location of the “hinge
267 zone” control the volume of ice lost from the East Antarctic Ice Sheet since the LGM.

268 An implication of this interior portion of the EAIS being thicker, rather than thinner, at the LGM is that the ice
269 subsequently thinned, allowing us to evaluate deglacial leads and lags between the coast and interior. The earliest
270 deglaciation constraints in this region come from ice-sheet thinning in the Prince Charles Mountains at 18 ka
271 (White *et al.*, 2011; Bentley *et al.*, 2014), which was possibly coincident with grounding-line retreat on the
272 continental shelf in Prydz Bay (Mackintosh *et al.*, 2014). Ice-shelf retreat began by ~16 ka and ~14 ka in west-
273 central and eastern Prydz Bay, respectively, with the Rauer Group and Vestfold Hills ice-free by ~11 ka (White
274 *et al.*, 2022). Our record of initial ice thinning in the Grove Mountains at ~15 ka indicates that thinning occurred
275 ~3 kyr earlier in the Prince Charles Mountains, though the timing at the Grove Mountains is broadly consistent



12

276 with available evidence of deglaciation at the coast. The modern ice-surface elevation was reached by 9-12 ka at
277 the Prince Charles Mountains (White *et al.*, 2011) but 1.4 ka in the Grove Mountains, ~7.6-10.6 ka later.
278 Deglaciation thus possibly started and likely finished earlier downstream, and the magnitude of thinning was
279 greater at the Antarctic coastline than in its interior. Ice-sheet modeling indicates that responses to sea-level rise,
280 decreased accumulation, and changes in temperature should manifest first at the margins of the ice sheet, causing
281 thinning to propagate into the interior of the ice sheet (Alley and Whillans, 1984; Spector *et al.*, 2019). Such
282 propagation is likely slowed and attenuated by distance and travel over bedrock highs (Johnson *et al.*, 2021), such
283 as the Grove Mountains. Modern observations confirm that such dynamic thinning occurs over decadal timescales
284 (e.g., Felikson *et al.*, 2017), but our data indicate that such processes may continue over centuries to millennia.
285 If the Grove Mountains are representative of the behavior of similar locations in interior East Antarctica, more of
286 the EAIS may have been thicker-than-present at the LGM and subsequent thinned than was previously thought.
287 Ice-sheet models may thus currently underestimate LGM ice volume and rates and magnitudes of deglacial ice
288 loss. Thicker-than-at-present LGM ice being limited to areas of East Antarctica within a few hundreds of
289 kilometers from the coastline would be consistent with reconstructions of MWP-1a that call for only a limited
290 input of meltwater from Antarctica (e.g., Yeung *et al.*, 2019). Our work shows that EAIS thickening extended
291 further inland than indicated by ¹⁰Be and ²⁶Al ages (e.g., Lilly *et al.*, 2010), providing a modest additional ice
292 volume for MWP-1a, and that thinning started before and possibly occurred during the period of MWP-1a. While
293 we cannot accurately quantify how much EAIS volume was lost during this period, our data indicate that likely
294 less than half of the post-LGM ice loss occurred before or during MWP-1a in this region, consistent with studies
295 identifying Antarctica as likely being a minor contributor and the majority of the Antarctic contribution to have
296 been sourced from West Antarctica (e.g., Lin *et al.*, 2021).

297 **5 Conclusions**

298 Our results using *in situ* ¹⁴C provide new and improved constraints on past East Antarctic Ice Sheet thickness at a
299 site ~400 km inland from the present-day coast. These data show that the ice sheet at the Grove Mountains was
300 thicker, not thinner, at the LGM, but the summits of these nunataks were exposed. Ice-sheet thinning began here
301 ~15 ka and continued through the Holocene, likely in response to changes near the grounding line that propagated
302 upstream. This work demonstrates that the LGM “hinge zone”—between thinner ice in the interior and thicker ice
303 at the coast relative to today—was further inland than was previously thought. The additional ice volume implied
304 by these findings therefore needs to be accounted for in numerical ice sheet and glacial isostatic adjustment
305 reconstructions of the last deglaciation.

306 **Code availability**

307 **Data availability**

308 All data described in the paper are included in Supplementary Table 1.

309 **Interactive computing environment**



13

310 **Sample availability**

311 **Video supplement**

312 **Author contributions**

313 CR processed samples for ^{14}C analysis, wrote the paper, and prepared all figures. CR, RJ, and AM conceived the
314 project. All authors read and commented on the manuscript. BG provided code for exposure-age calculation and
315 plotting. KL undertook fieldwork in the Grove Mountains and collected all the field observations and samples
316 presented here.

317 **Competing interests**

318 The authors declare that they have no conflict of interest.

319 **Disclaimer**

320 **Acknowledgements**

321 This work was supported by Australian Research Council grants DE210101923, awarded to RSJ, and ARC
322 Special Research Initiative ‘Securing Antarctica’s Environmental Future’ (SR200100005). CR would also like to
323 acknowledge support from the Monash Graduate and International Tuition Scholarships.

324 **References**

- 325 Alley, R. B. and Whillans, I. M.: Response of the East Antarctica ice sheet to sea-level rise, *Journal of Geophysical*
326 *Research: Oceans*, 89, 6487-6493, 1984.
- 327 Andersen, J. L., Newall, J. C., Fredin, O., Glasser, N. F., Lifton, N. A., Stuart, F. M., Fabel, D., Caffee, M.,
328 Pedersen, V. K., and Koester, A. J.: A topographic hinge-zone divides coastal and inland ice dynamic regimes in
329 East Antarctica, *Communications Earth & Environment*, 4, 9, 2023.
- 330 Balco, G., Stone, J. O., Sliwinski, M. G., and Todd, C.: Features of the glacial history of the Transantarctic
331 Mountains inferred from cosmogenic ^{26}Al , ^{10}Be and ^{21}Ne concentrations in bedrock surfaces, *Antarctic Science*,
332 26, 708-723, 2014.
- 333 Bentley, M. J., Cofaigh, C. O., Anderson, J. B., Conway, H., Davies, B., Graham, A. G., Hillenbrand, C.-D.,
334 Hodgson, D. A., Jamieson, S. S., and Larter, R. D.: A community-based geological reconstruction of Antarctic
335 Ice Sheet deglaciation since the Last Glacial Maximum, *Quaternary Science Reviews*, 100, 1-9, 2014.
- 336 Bindschadler, R., H. Choi, and ASAID Collaborators. 2011. High-resolution Image-derived Grounding and
337 Hydrostatic Lines for the Antarctic Ice Sheet. Boulder, Colorado, USA: National Snow and Ice Data Center.
338 Digital media.
- 339 Bockheim, J. G., Wilson, S. C., Denton, G. H., Andersen, B. G., and Stuiver, M.: Late quaternary ice-surface
340 fluctuations of Hatherton Glacier, Transantarctic Mountains, *Quaternary Research*, 31, 229-254, 1989.



- 341 Buizert, C., Fudge, T., Roberts, W. H., Steig, E. J., Sherriff-Tadano, S., Ritz, C., Lefebvre, E., Edwards, J.,
342 Kawamura, K., and Oyabu, I.: Antarctic surface temperature and elevation during the Last Glacial Maximum,
343 *Science*, 372, 1097-1101, 2021.
- 344 Burton-Johnson, A., Black, M., Fretwell, P. T., and Kaluza-Gilbert, J.: An automated methodology for
345 differentiating rock from snow, clouds and sea in Antarctica from Landsat 8 imagery: a new rock outcrop map
346 and area estimation for the entire Antarctic continent, *The Cryosphere*, 10, 1665-1677, 2016.
- 347 Coulon, V., Bulthuis, K., Whitehouse, P. L., Sun, S., Haubner, K., Zipf, L., and Pattyn, F.: Contrasting response
348 of West and East Antarctic ice sheets to glacial isostatic adjustment, *Journal of Geophysical Research: Earth*
349 *Surface*, 126, e2020JF006003, 2021.
- 350 DeConto, R. M., Pollard, D., Alley, R. B., Velicogna, I., Gasson, E., Gomez, N., Sadai, S., Condron, A., Gilford,
351 D. M., and Ashe, E. L.: The Paris Climate Agreement and future sea-level rise from Antarctica, *Nature*, 593, 83-
352 89, 2021.
- 353 Deschamps, P., Durand, N., Bard, E., Hamelin, B., Camoin, G., Thomas, A. L., Henderson, G. M., Okuno, J. i.,
354 and Yokoyama, Y.: Ice-sheet collapse and sea-level rise at the Bølling warming 14,600 years ago, *Nature*, 483,
355 559-564, 2012.
- 356 Dunai, T. J.: *Cosmogenic nuclides: principles, concepts and applications in the earth surface sciences*, Cambridge
357 University Press, 2010.
- 358 Felikson, D., Bartholomaus, T. C., Catania, G. A., Korsgaard, N. J., Kjær, K. H., Morlighem, M., Noël, B., Van
359 Den Broeke, M., Stearns, L. A., and Shroyer, E. L.: Inland thinning on the Greenland ice sheet controlled by outlet
360 glacier geometry, *Nature Geoscience*, 10, 366-369, 2017.
- 361 Fogwill, C., Turney, C., Gолledge, N., Rood, D., Hippe, K., Wacker, L., Wieler, R., Rainsley, E., and Jones, R.:
362 Drivers of abrupt Holocene shifts in West Antarctic ice stream direction determined from combined ice sheet
363 modelling and geologic signatures, *Antarctic Science*, 26, 674-686, 2014.
- 364 Goehring, B. M., Balco, G., Todd, C., Moening-Swanson, I., and Nichols, K.: Late-glacial grounding line retreat
365 in the northern Ross Sea, Antarctica, *Geology*, 47, 291-294, 2019.
- 366 Goehring, B. M., Wilson, J., and Nichols, K.: A fully automated system for the extraction of in situ cosmogenic
367 carbon-14 in the Tulane University cosmogenic nuclide laboratory, *Nuclear Instruments and Methods in Physics*
368 *Research Section B: Beam Interactions with Materials and Atoms*, 455, 284-292, 2019.
- 369 Hanna, E., Pattyn, F., Navarro, F., Favier, V., Goelzer, H., van den Broeke, M. R., Vizcaino, M., Whitehouse, P.
370 L., Ritz, C., and Bulthuis, K.: Mass balance of the ice sheets and glaciers—Progress since AR5 and challenges,
371 *Earth-Science Reviews*, 201, 102976, 2020.
- 372 Hillebrand, T. R., Stone, J. O., Koutnik, M., King, C., Conway, H., Hall, B., Nichols, K., Goehring, B., and
373 Gillespie, M. K.: Holocene thinning of Darwin and Hatherton glaciers, Antarctica, and implications for grounding-
374 line retreat in the Ross Sea, *The Cryosphere*, 15, 3329-3354, 2021.
- 375 Hippe, K. and Lifton, N. A.: Calculating isotope ratios and nuclide concentrations for in situ cosmogenic ¹⁴C
376 analyses, *Radiocarbon*, 56, 1167-1174, 2014.
- 377 Johnson, J. S., Pollard, D., Whitehouse, P. L., Roberts, S. J., Rood, D. H., and Schaefer, J. M.: Comparing glacial-
378 geological evidence and model simulations of ice sheet change since the last glacial period in the Amundsen Sea
379 sector of Antarctica, *Journal of Geophysical Research: Earth Surface*, 126, e2020JF005827, 2021.



- 380 Jones, R. S., Johnson, J. S., Lin, Y., Mackintosh, A. N., Sefton, J. P., Smith, J. A., Thomas, E. R., and Whitehouse,
381 P. L.: Stability of the Antarctic Ice Sheet during the pre-industrial Holocene, *Nature Reviews Earth &*
382 *Environment*, 3, 500-515, 2022.
- 383 Lifton, N., Sato, T., and Dunai, T. J.: Scaling in situ cosmogenic nuclide production rates using analytical
384 approximations to atmospheric cosmic-ray fluxes, *Earth and Planetary Science Letters*, 386, 149-160, 2014.
- 385 Lilly, K.: Three million years of East Antarctic ice sheet history from in situ cosmogenic nuclides in the Lambert-
386 Amery Basin, 2008. 2008.
- 387 Lilly, K., Fink, D., Fabel, D., and Lambeck, K.: Pleistocene dynamics of the interior East Antarctic ice sheet,
388 *Geology*, 38, 703-706, 2010.
- 389 Lin, Y., Hibbert, F. D., Whitehouse, P. L., Woodroffe, S. A., Purcell, A., Shennan, I., and Bradley, S. L.: A
390 reconciled solution of Meltwater Pulse 1A sources using sea-level fingerprinting, *Nature communications*, 12,
391 2015, 2021.
- 392 Liu, H., K. C. Jezek, B. Li, and Z. Zhao. 2015. Radarsat Antarctic Mapping Project Digital Elevation Model,
393 Version 2. [Indicate subset used]. Boulder, Colorado USA. NASA National Snow and Ice Data Center Distributed
394 Active Archive Center. doi: <http://dx.doi.org/10.5067/8JKNEW6BFRVD>. [Accessed 1/08/2023]
- 395 Mackintosh, A., White, D., Fink, D., Gore, D. B., Pickard, J., and Fanning, P. C.: Exposure ages from mountain
396 dipsticks in Mac. Robertson Land, East Antarctica, indicate little change in ice-sheet thickness since the Last
397 Glacial Maximum, *Geology*, 35, 551-554, 2007.
- 398 Mackintosh, A. N., Verleyen, E., O'Brien, P. E., White, D. A., Jones, R. S., McKay, R., Dunbar, R., Gore, D. B.,
399 Fink, D., and Post, A. L.: Retreat history of the East Antarctic Ice Sheet since the last glacial maximum,
400 *Quaternary Science Reviews*, 100, 10-30, 2014.
- 401 Matsuoka, K., Skoglund, A., Roth, G., de Pomereu, J., Griffiths, H., Headland, R., ... Melvær, Y. (2018).
402 Quantarctica [Data set]. Norwegian Polar Institute. <https://doi.org/10.21334/npolar.2018.8516e961>
- 403 Miles, B. W., Stokes, C. R., Jenkins, A., Jordan, J. R., Jamieson, S. S., and Gudmundsson, G. H.: Slowdown of
404 Shirase Glacier, East Antarctica, caused by strengthening alongshore winds, *The Cryosphere*, 17, 445-456, 2023.
- 405 Nichols, K. A. and Goehring, B. M.: Isolation of quartz for cosmogenic in situ ¹⁴C analysis, *Geochronology*, 1,
406 43-52, 2019.
- 407 Nichols, K. A., Goehring, B. M., Balco, G., Johnson, J. S., Hein, A. S., and Todd, C.: New last glacial maximum
408 ice thickness constraints for the Weddell Sea Embayment, Antarctica, *The Cryosphere*, 13, 2935-2951, 2019.
- 409 Nichols, K. A.: A decade of in situ cosmogenic ¹⁴C in Antarctica, *Annals of Glaciology*, 2022. 1-6, 2022.
- 410 Rignot, E., Mouginot, J., and Scheuchl, B.: Ice flow of the Antarctic ice sheet, *Science*, 333, 1427-1430, 2011.
- 411 Rignot, E., Mouginot, J., Scheuchl, B., Van Den Broeke, M., Van Wessem, M. J., and Morlighem, M.: Four
412 decades of Antarctic Ice Sheet mass balance from 1979–2017, *Proceedings of the National Academy of Sciences*,
413 116, 1095-1103, 2019.
- 414 Spector, P., Stone, J., and Goehring, B.: Thickness of the divide and flank of the West Antarctic Ice Sheet through
415 the last deglaciation, *The Cryosphere*, 13, 3061-3075, 2019.
- 416 Stokes, C. R., Abram, N. J., Bentley, M. J., Edwards, T. L., England, M. H., Foppert, A., Jamieson, S. S., Jones,
417 R. S., King, M. A., and Lenaerts, J.: Response of the East Antarctic Ice Sheet to past and future climate change,
418 *Nature*, 608, 275-286, 2022.



- 419 Walker, M., Johnsen, S., Rasmussen, S. O., Popp, T., Steffensen, J. P., Gibbard, P., Hoek, W., Lowe, J., Andrews,
420 J., and Björck, S.: Formal definition and dating of the GSSP (Global Stratotype Section and Point) for the base of
421 the Holocene using the Greenland NGRIP ice core, and selected auxiliary records, *Journal of Quaternary Science*:
422 Published for the Quaternary Research Association, 24, 3-17, 2009.
- 423 White, D., Fülöp, R.-H., Bishop, P., Mackintosh, A., and Cook, G.: Can in-situ cosmogenic ¹⁴C be used to assess
424 the influence of clast recycling on exposure dating of ice retreat in Antarctica?, *Quaternary Geochronology*, 6,
425 289-294, 2011.
- 426 White, D. A., Fink, D., and Gore, D. B.: Cosmogenic nuclide evidence for enhanced sensitivity of an East
427 Antarctic ice stream to change during the last deglaciation, *Geology*, 39, 23-26, 2011.
- 428 White, D. A., Fink, D., Lilly, K., O'Brien, P., Dorschel, B., Berg, S., Bennike, O., Gore, D. B., Fabel, D., and
429 Blaxell, M.: Rapid ice sheet response to deglacial and Holocene paleoenvironmental changes in eastern Prydz
430 Bay, East Antarctica, *Quaternary Science Reviews*, 280, 107401, 2022.
- 431 Yamane, M., Yokoyama, Y., Miura, H., Maemoku, H., Iwasaki, S., and Matsuzaki, H.: The last deglacial history
432 of Lützow-Holm Bay, East Antarctica, *Journal of Quaternary Science*, 26, 3-6, 2011.
- 433 Yeung, N., Menviel, L., Meissner, K., and Sikes, E.: Assessing the Spatial Origin of Meltwater Pulse 1A Using
434 Oxygen-Isotope Fingerprinting, *Paleoceanography and Paleoclimatology*, 34, 2031-2046, 2019.
- 435 Zwally, H. Jay, Mario B. Giovinetto, Matthew A. Beckley, and Jack L. Saba, 2012, Antarctic and Greenland
436 Drainage Systems, GSFC Cryospheric Sciences Laboratory, at
437 http://icesat4.gsfc.nasa.gov/cryo_data/ant_grn_drainage_systems.php